Towards High Activity of Hydrogen production from Ammonia Borane over Efficient Non-noble Ni_5P_4 Catalyst

Xiang Feng[†*], Yuhai Zhao[†], Dakuo Liu[†], Yasi Mo[†], Yibin Liu[†], Xiaobo Chen[†], Wenjuan Yan[†], Xin Jin[†], Bingxu Chen[§], Xuezhi Duan[§], De Chen[‡], Chaohe Yang[†]

[†]*State Key Laboratory of Heavy Oil Processing, China University of Petroleum, 66 Changjiang Road, Qingdao 266580, China*

[‡] *Department of Chemical Engineering, Norwegian University of Science and Technology, Trondheim 7491, Norway*

[§] *State Key Laboratory of Chemical Engineering, East China University of Science and Technology, Shanghai 200237, China.*

* Corresponding author: xiangfeng@upc.edu.cn, Tel/Fax: +86 053286984710

Abstract: Catalytic hydrolysis of ammonia borane has tremendous potential as an energy-efficient approach to supply hydrogen for energy vehicles and portable electronic devices. Herein, DFT calculation is first performed on electronic properties of Ni_2P and Ni_5P_4 nanocatalysts. It is found that more electrons are transferred from Ni to P for Ni_5P_4, indicating that Ni_5P_4 may show superior performance based on the electron effect. Therefore, Ni_2P and Ni_5P_4 with high purity are synthesized by the phase-controlled thermal decomposition approach. Gratifyingly, the Ni_5P_4 catalyst exhibits the as-expected better catalytic activity than that of Ni_2P catalyst. It also shows low activation energy and good stability. Furthermore, the structures and morphologies of both catalysts are characterized by multi-techniques such as XRD, HRTEM and XPS. The better performance could be ascribed to the higher positive charge of Ni together with the stronger ensemble effect of P. The insights sheds new light on the design of efficient Ni-P catalysts for hydrogen generation.

Keywords: Ammonia borane; Catalytic hydrolysis; Electron transfer; Nickel phosphide

Introduction

The ever-increasing demand for clean energy and concern for environment trigger the rapid development of alternative sustainable energy. Hydrogen, as a clean energy carrier, shows a significantly higher gravimetric energy density (120 kJ/g) than that of petroleum (44 kJ/g)[1]. It can be renewably produced from non-fossil feedstocks[2]. Although hydrogen shows obvious advantages such as energetic and clean, it still has drawbacks[3] in the storage, purification and production processes. Hydrogen storage is especially problematic, which imposes a scientific and technological challenge to researchers.

In order to address the above concerns, hydrogen generation from hydrogen storage materials offers the convenient, effective and cost-efficient approach[4-7]. The leading contender for chemical hydrogen-storage materials is ammonia-borane (NH_3BH_3, AB)[8-10]. It has the following advantages: 1) high hydrogen content (19.6 wt%) which is much higher than the targeted value (5.5 wt%) for the year 2020 set by the US Department of Energy; 2) low molecular weight (30.87 g/mL) and high volumetric density of 146 g/L; 3) high solubility in H_2O, long-term stability in aqueous solutions and air at room temperature and 4) non-toxicity. These characteristics have provoked tremendous research on AB hydrolysis.

Xu et al. first found that transition metals are active for AB hydrolysis[11]. Since then, many precious metals such as platinum[12, 13], rhodium[14, 15] and ruthenium[16] have been demonstrated to show high catalytic performance and low activation energy for AB hydrolysis. However, the high cost of precious metal has limited its commercial application. One scenario to solve this problem is to maximize the turnover frequency

of precious metal, such as reducing the nanoparticle size. For example, we systematically studied the size-dependence of Pt nanoparticle and greatly improved the performance[17]. Recently, Yan et al. employed the bottom-up precise method to synthesize stable platinum dimers on graphene, and achieved high specific rate of 2800 molH_2/mol$_{Pt}$/min at room temperature[18]. Another scenario is to use cost-effective non-precious metal to replace precious metal catalysts. To this end, nonprecious catalyst (e.g., nickel, iron, cobalt, copper) were reported to exhibit remarkable activities in the hydrolytic dehydrogenation of AB[19-22]. Fu et al. first reported that Ni_2P could show good performance for AB hydrolysis[23]. It is noted that the nickel phosphate-based material could have different phases and may affect the performance of AB hydrolysis. Therefore, developing new nickel phosphate-based material and elucidate the effect of P on performance is highly desired to the design of efficient Ni-based catalyst for AB hydrolysis.

In this work, we first performed DFT calculation on electronic properties of Ni_2P and Ni_5P_4 catalysts. Results show that more electrons can be transferred from Ni to P for Ni_5P_4 catalyst. Based on the electronic effect for AB hydrolysis, it is estimated that Ni_5P_4 may show superior performance. Therefore, Ni_2P and Ni_5P_4 are experimentally synthesized by the phase-controlled thermal decomposition approach. Multi-techniques such as X-ray diffraction (XRD), transmission electron microscopy (TEM) and X-ray photoelectron spectroscopy (XPS) are employed to investigate the structure and morphology of the catalysts. Notably, the Ni_5P_4 catalyst exhibits the as-expected better catalytic activity than that of Ni_2P catalyst. This could be ascribed to the electronic effect (i.e., higher positive charge of Ni) together with the stronger ensemble effect of P. The results are of great referential importance to the design of efficient nickel phosphide catalysts for hydrogen generation.

Experimental Section

Chemicals

All chemicals were purchased from sinopharm chemical reagent unless otherwise indicated. The chemicals include ammonia borane ($NH_3 \cdot BH_3$, 97%), nickel(II) acetylacetonate (95%), nickel(II) nitrate hexahydrate (≥98%), 1-octadecene (ODE, 95%), oleylamine (OAm, 70%), trioctylphosphine (TOP, 97%), hexane (≥99%), ethanol (96 vol%), cerium(IV) oxide (Sigma-Aldrich, 99.9995%) and carbon nanotube (CNano Technology Ltd). Deionized water (DI, 18.2 MΩ·cm) was used in all experiments. All chemicals were used as received without further purification.

Synthesis of Ni_2P and Ni_5P_4 catalysts

In a typical process[24], $Ni(acac)_2$, OAm (21.3 mmol) and ODE (14.1 mmol) were placed in a four-neck flask and vigorously stirred under argon atmosphere. The mixture was heated to 120^{o}C and maintained for 30 min to remove dissolved oxygen and moisture. Afterwards, TOP was rapidly injected into the above solution, followed by heating to 320^{o}C for 2 h. The products were subsequently obtained by adding excess ethanol and separated by centrifugation at 4000 rpm for 10 min. The black precipitate was washed with a mixture of hexane and ethanol for three times to remove excess surfactant and organic solvent, and then placed in vacuum at 60^{o}C for 24 h. The molar ratios of the P : Ni precursor were 2.18 and 8.75 for Ni_2P and Ni_5P_4, respectively.

Synthesis of Ni, Ni/CeO_2 and Ni/CNTs catalysts

The Ni/CeO_2 and Ni/CNTs catalysts with same loading of 10wt% were prepared by incipient wetness impregnation method as follows. In a typical process, 1 g CNTs or CeO_2 support was added in required volume of $Ni(NO_3)_2$ aqueous solution at room

temperature. After vigorously stirring for 30 min, 5 wt% $NaBH_4$ solution was added to reduce Ni/CNTs or Ni/CeO_2 catalysts. The resulted products were filtered and washed with de-ionized H_2O for three times to remove the by-products and residual ions. The as-obtained catalysts were then dried under vacuum at 50^oC overnight. Ni catalyst is synthesized by $NaBH_4$ reduction of $Ni(NO_3)_2$ aqueous solution at room temperature.

Catalyst characterization

The crystal phases of Ni_2P and Ni_5P_4 catalysts were determined by X-ray diffraction (XRD, Rigaku D/Max2550VB/PC, Cu K_α radiation). The structure and shape of catalysts were obtained by high-resolution transmission electron microscopy (HRTEM) on a JEOL JSM-2010. The samples for TEM analysis were first prepared by sonicating in hexane. Subsequently, the mixture was deposited on an copper grid, which was slowly dried at ambient conditions. The binding energy of Ni was determined by x-ray photoelectron spectroscopy (XPS) analysis on a PHI5000Versa Probe spectrometer with monochromatic Al Kα radiation (hν=1486.6 eV). Before XPS analysis, the samples were first stored under Ar atmosphere. The binding energy of C_{1s} (284.6 eV) was used as a reference to correct the binding energy of the Ni-based catalysts. The spectra of Ni and P were deconvolution by XPSPEAK 4.1 with 80% Lorentzian-20% Gaussian peaks.

Catalytic testing

In a typical water-displacement method, the catalytic activity of AB hydrolysis over Ni NP catalysts was evaluated by on-line recording of the hydrogen volume in a water-filled measuring cylinder system according to our previous report[17]. A weighed catalyst and Teflon-coated stirring bar were first placed in a three-necked glass container under stirring. This container inside water bath was connected via the gas

outlet to a water-filled measuring cylinder. The water bath was used to keenly change the reaction temperature. Subsequently, 5 mL AB solution (0.01g/mL) was introduced into the glass container by a syringe. Water was then displaced by the evolved hydrogen, the amount of which was determined by an electronic balance. The calculation of TOF is shown in supporting information. All experiments are well-repeated at least three times and the results are reproducible.

Calculation methods

The density functional theory (DFT) calculation on the electronic properties of Ni_2P and Ni_5P_4 catalysts was carried out with the DMol3 program package in Materials Studio. The unit cells of bulk Ni_2P and Ni_5P_4 were built based on crystallographic data reported in literature[25]. The Ni_2P and Ni_5P_4 geometry were optimized under three dimensional periodic boundary conditions to further refine the structure. Considering the electronic polarization effect, the double-numerical plus polarization (DNP) basis set with a real space cutoff radius of 4.5 Å and PW91 exchange-correlation functional were used according to literature[26]. The SCF tolerance was set as $1.0*10^{-6}$ Ha, and spin-unrestricted approach was used for all models. The atomic charges of the Ni_2P and Ni_5P_4 were obtained by the popular charge analysis methods, i.e., the Mulliken analysis, which was based on projecting the occupied one-electron eigenstates onto a localized basis set[27, 28].

Results and discussion

It was reported that Ni_2P could show good performance for many reactions, such as AB hydrolysis[23, 29, 30], direct formic acid fuel cells[31] and hydrogen evolution reaction (HER)[24] because of the unique properties originated from the addition of P.

Herein, the electronic interaction between Ni and P is first investigated by DFT calculation. The geometries (Figure 1) of bulk Ni_2P and Ni_5P_4 model were built according to experimental lattice parameters[25]. For Ni_2P, the parameters are a=b=0.5859 nm and c=0.3382 nm. In contrast, the parameters for Ni_5P_4 are a=b=0.679 and c=1.099. Relatively large phosphorus is well accommodated using the trigonal prisms structure of this metal-rich phosphides. It can be seen from Table 1 that the optimized structural parameters of both Ni_2P and Ni_5P_4 coincide well with the experimental data and literature[25, 26, 32, 33], indicating the correctness of models.

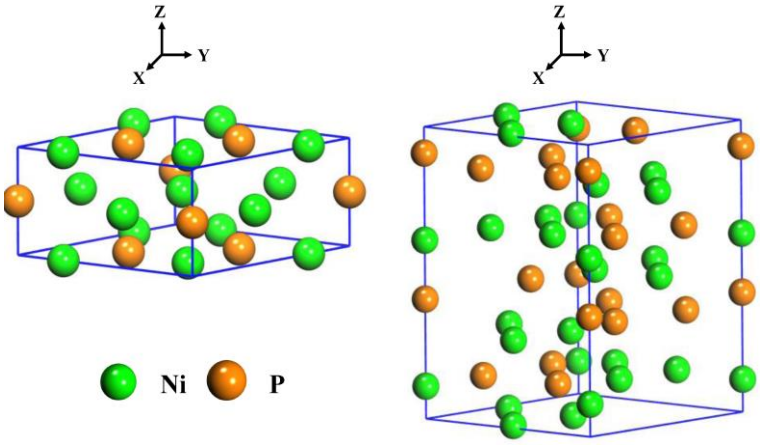

Figure 1 Unit cell of Ni_2P (left) and Ni_5P_4 (right) material.

Table 1 Experimental and theoretical structural parameters of Ni_2P and Ni_5P_4.

Sample	nm	Theoretical	Experimental[25, 32, 33]
Ni_2P	a	0.587	0.586
Ni_2P	c	0.337	0.338
Ni_5P_4	a	0.679	0.679
Ni_5P_4	c	1.100	1.099

The Mulliken charge analysis is then performed, and the results are shown in Figure 2. For Ni_2P the average charge per Ni atom after introduction of P is 0.038 e. This positive charge of Ni shows that there is electron transfer from Ni to P. In comparison, the average charge per Ni atom for Ni_5P_4 is 0.119 e. This larger value shows that electron on Ni_5P_4 is more easily to be transferred from Ni to P than on Ni_2P. It is reported that the catalytic activity for AB hydrolysis can be greatly affected by the metal electronic properties[17]. For example, metal nanoparticle (e.g., Pt) that donates electron to support exhibits significantly increased hydrogen generation rate than Pt catalyst that receives electron. Therefore, based on this electronic effect, it is thus expected that Ni_5P_4 material with more electron transfer from Ni to P may exhibit higher TOF ($mol_{H2}/mol_{cat}/min$).

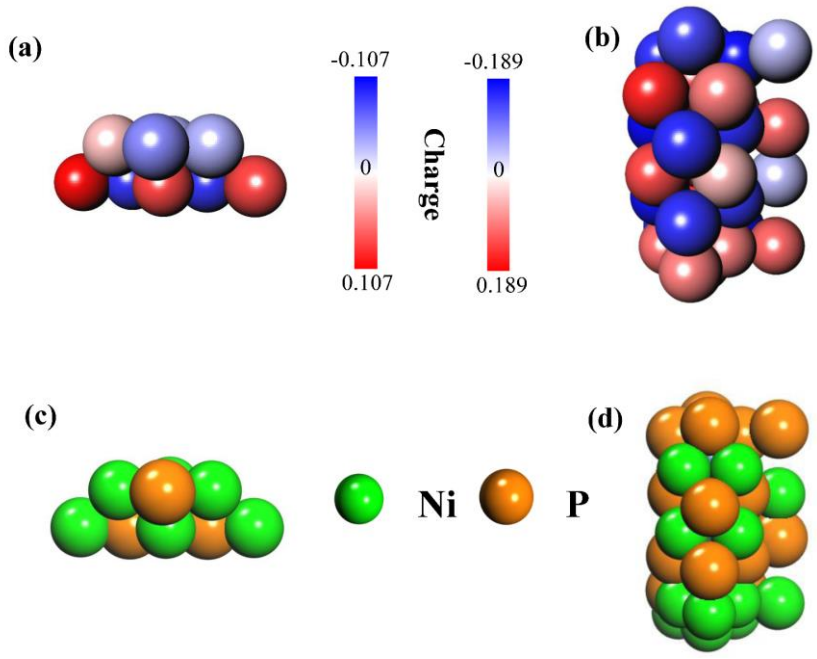

Figure 2 Charge analysis of bulk Ni_2P and Ni_5P_4 materials. The blue and red colors indicate the charge labeled in the color map, where blue and red value means receiving or donating electrons, respectively. The figure 2(c-d) are shown to distinguish the Ni and P atoms.

The crystalline phase structure and the purity of the as-synthesized nickel phosphide (i.e., Ni_2P and Ni_5P_4) catalysts are characterized by XRD, as shown in Figure 3. When the P/Ni ratio is 2.18, Ni_2P phase with high purity was obtained. The intense diffraction peaks at 40.8, 44.7, 47.5, 54.4, 66.4 are attributed to the (111), (201), (210), (300), (310) crystal facets, respectively. These diffraction peaks are in accordance with the hexagonal structure of Ni_2P (PDF#03-065-3544). No extra peaks are clearly observed in this range, indicating the high purity of Ni_2P phase. Higher P/Ni ratio of 8.75 results in the presence of Ni_5P_4 phase. The hexagonal structure of Ni_5P_4 matches well with all diffraction peaks (PDF # 03-065-2075). The intense diffraction peaks at 28.8, 30.4, 31.5, 34.7, 36.1, 40.6, 41.4, 46.3, 47.0, 47.9, 49.9, 53.1 and 54.1 are attributed to the (103), (200), (201), (202), (104), (210), (211), (300), (301), (213), (006), (303) and (220) crystalline phases, respectively. No other obvious extraneous peaks exist, confirming the purity of crystal. These XRD results show that both of Ni_2P and Ni_5P_4 have high crystallinity and purity, which are required to elucidate the electronic effect and structure-performance relationship for AB hydrolysis.

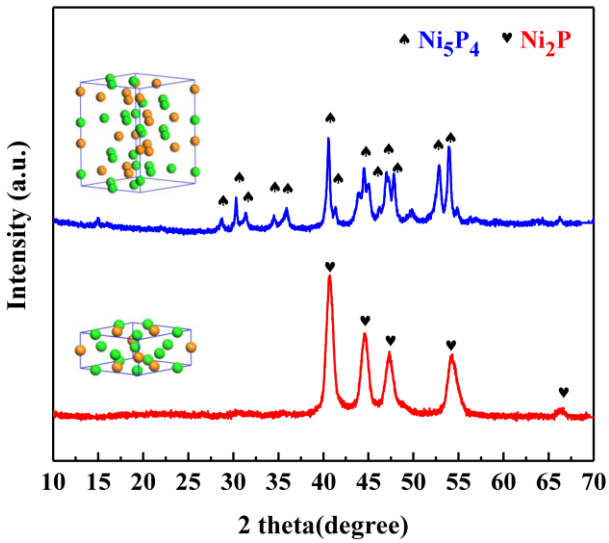

Figure 3 XRD patterns of Ni_2P and Ni_5P_4 catalysts.

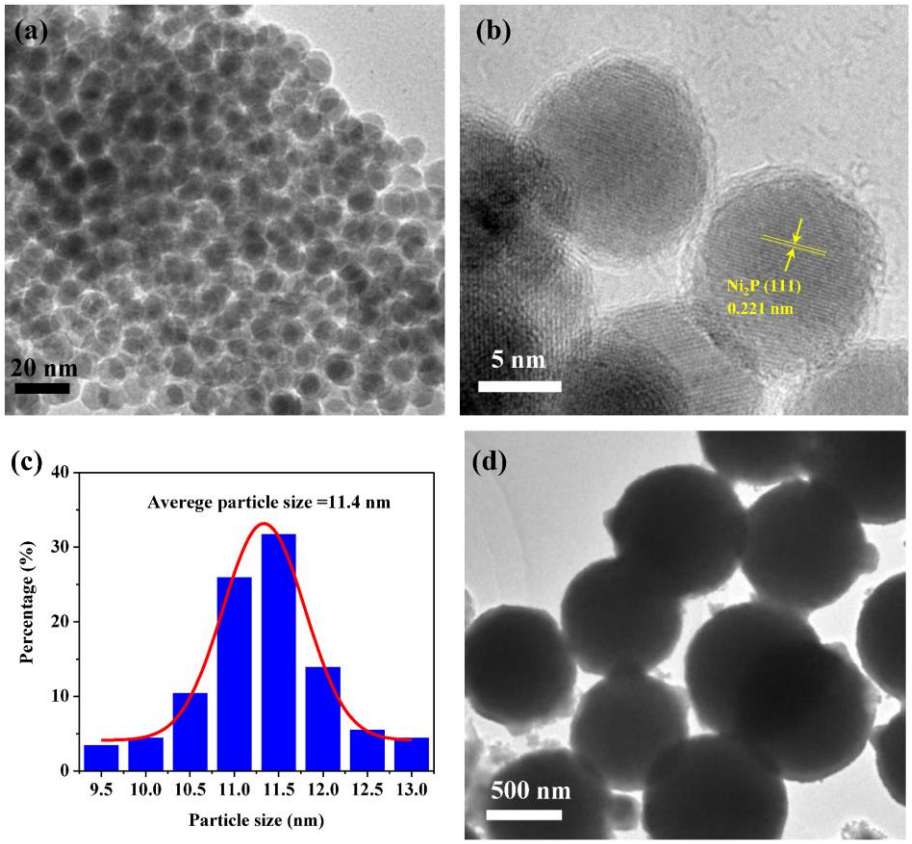

Figure 4 Representative HRTEM images of nickel phosphide different phases of Ni_2P (a-b) and Ni_5P_4 (d), and particle size distribution of Ni_2P catalyst (c).

Figure 4 and Figure S1-S2 show the representative TEM images of Ni_2P and Ni_5P_4 catalysts. It can be seen that the Ni_2P shows regular solid spherical shape with average particle size of ca. 11 nm. The HRTEM image (Fig. 4b) reveals that the fringe spacing is about 0.221nm. This corresponds to the (111) lattice plane of hexagonal Ni_2P, which coincides well with the XRD results in Figure 3. Fig. 4d shows the morphology of the Ni_5P_4 catalyst. It can be seen that only big solid spheres are obtained, and the average particle size is ca. 800 nm (Figure S3). This can be explained by the nickel phosphate formation mechanism[24]. In the synthesis process, nickel nanoclusters can be first formed using OAm as the reductant when the reaction temperature reaches 200°C. Subsequently, P precursor (i.e., TOP) can strongly adsorb on the surface of Ni, forming

the Ni-TOP complexes [24]. With the gradual increase of reaction temperature to 320°C, the phosphorus is formed by the breaking of P-C bond. The as-formed phosphorus can therefore diffuse into the Ni nanoclusters, forming Ni_2P and Ni_5P_4 nanoparticles. When the Ni/P ratio is high (i.e., Ni_2P), the inward diffusion of phosphorus atoms is larger than the outward diffusion, and thus generates small solid Ni_2P nanoparticle. When the Ni/P ratio is smaller for Ni_5P_4, a similar diffusion speed of nickel and phosphorus is reached, resulting in steady state in all directions of the particle. Because of the high surface energy and intermolecular forces of the unstable solid nanoparticle, the aggregation of Ni_5P_4 into solid spheres occurs. These results confirm that the crystal phase of nickel phosphide can be controlled by carefully modifying the Ni/P ratio.

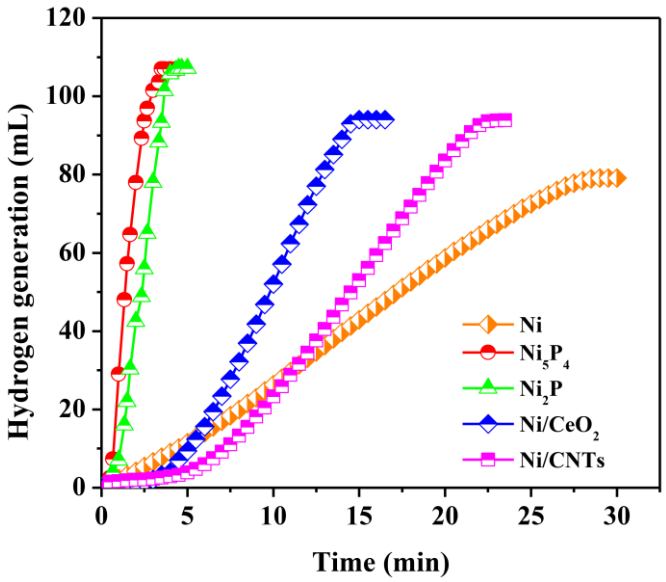

Figure 5 Catalytic activity of different Ni-based catalysts with same weight of 0.038g. Reaction conditions: 25°C, C_{AB}=0.01g/mL, V_{AB}=5mL.

The catalytic performance of Ni_2P and Ni_5P_4 catalysts are therefore tested for AB hydrolysis (Figure 5). AB hydrolysis reaction is depicted as the following equation, $NH_3BH_3 + 4H_2O \rightarrow NH_4^+ + B(OH)_4^- + 3H_2$[20]. Therefore, the maximum value of 3mol

H_2 can be generated with 1mol of NH_3BH_3 for each experiment. It can be seen that only less than 100 mL of hydrogen can be generated in 14, 22 and 28 min for Ni/CeO_2, Ni/CNTs and Ni catalyst, respectively. In sharp contrast, the Ni_2P catalyst can generate total amount of hydrogen in ca. 3 min. Compared with Ni_2P catalyst, Ni_5P_4 shows as expected higher activity, with generation of all hydrogen in shorter time. The calculated TOF for Ni_5P_4 and Ni_2P is 23.5 and 6.3 $mol_{H2}/min/mol_{cat}$, respectively.

Normally, smaller Ni_xP_y particle size leads to better performance. However, Ni_5P_4 with larger particle size still shows higher TOF than Ni_2P. Therefore, size effect should not be the dominate reason. The electronic properties of the two catalysts are further studied. The chemical states of Ni and P elements for Ni_2P and Ni_5P_4 catalysts are studied by XPS. Figure 6a shows the Ni $2p_{3/2}$ and Ni $2p_{1/2}$ regions, which consist of spin-orbit doublets and shakeup satellite peaks. In the Ni $2p_{3/2}$ region of Ni_2P sample, the three peaks with binding energy (BE) of 852.6, 855.9 and 860.8 eV are ascribed to the $Ni^{\delta+}$[34, 35], Ni(II) from superficial oxidation of Ni_2P[36] and satellite peak of Ni $2p_{3/2}$[37], respectively. In addition, the $Ni^{\delta+}$ in Ni_2P, oxidized Ni species and satellite peak of Ni $2p_{1/2}$ region are found at 869.9, 873.7 and 878.6eV. Compared with Ni_2P, the three corresponding peaks of Ni $2p_{3/2}$ are observed at 852.9, 856.2 and 861.3 eV for Ni_5P_4. It can be seen that there is positive shift of BE for each peak of Ni_5P_4 catalyst. For example, the $Ni^{\delta+}$ shifts from 852.6 to 852.9 eV for Ni_5P_4 catalyst. This positive shift for Ni_5P_4 shows that Ni donates more electron, which is in accordance with the DFT calculation in Figure 2. Figure 6b and 6d show the P 2p region of Ni_2P and Ni_5P_4 catalysts. For Ni_2P catalyst, the peaks at 129.0 and 130.0 are assigned to P $2p_{1/2}$ and P $2p_{3/2}$ in Ni_2P, respectively[38], and the peak at 133.2 eV is ascribed to oxidized P species. In comparison, the P 2p peaks of Ni_5P_4 show negative shifts. The corresponding peaks are observed at 128.7, 129.6 and 132.7 eV. The negative shift of P2p peaks

together with positive shifts of Ni 2p peaks confirm the DFT calculation

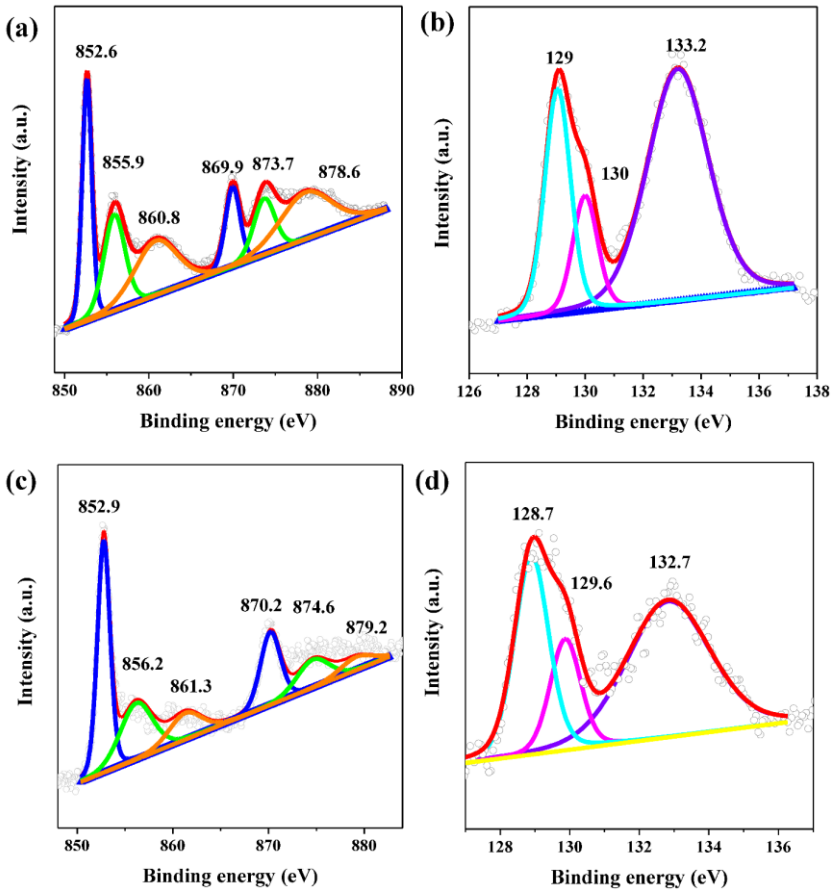

Figure 6 XPS spectra of Ni 2p and P 2p for Ni_2P (a, b) and Ni_5P_4 (c, d) catalysts.

results that more electron are transferred from Ni to P for Ni_5P_4 catalyst. The electron-deficient metal sites are favor for the adsorption of B-H in AB molecule, forming and breaking M-H bond to generate H_2. Therefore, this should be one reason for the enhanced catalytic activity for Ni_5P_4 catalyst towards AB hydrolysis. Besides enhanced electron transfer on Ni_5P_4 catalyst, it is worth noting that the ensemble effect of P could also be beneficial for improving the catalytic activity. The contents of P in Ni_5P_4 (44 at% P) is actually larger than that in Ni_2P (33 at% P). In addition, the Ni/P ratio determined from XPS is also quite similar to the stoichiometric ratio. Therefore, this ensemble effect reduces the number of Ni active sites, decreasing the energy cost

for H_2 removal from nickel phosphate catalyst.

The catalytic activity of Ni_5P_4 catalyst is subsequently evaluated at different temperature with smaller n_{Cat}/n_{AB} ratio of 0.02 (Figure 7a). With the increase of reaction temperature from 25 to 50 ^oC, the TOF can be further increased to 53 $mol_{H2}/min/mol_{cat}$. This observation agrees well with previously reported results that high temperature is favorable for the hydrogen generation in AB hydrolysis. Compared with literature (Figure 7b)[38-40], the TOF of Ni_5P_4 at 25^oC (Figure 5) is quite impressive. It is even higher than some of precious catalysts[41-44], such as Ir-PNP, Sn-Pd/C and Pt-Ni@SiO_2. It should be noted increasing the n_{Cat}/n_{AB} ratio or changing AB concentration could further enhance the activity[23, 29]. However, the aim of this paper is to propose a strategy to modify catalytic performance by manipulating electron transfer for nickel phosphate catalyst. Therefore, further enhancing performance by other methods such as adding promoter, studying size effect or optimizing reaction conditions are interesting topics, which may be taken in our future study.

The temperature dependent TOF can be used to evaluate the activation energy (i.e., E_a) by Arrhenius equation (3-1):

$$r = r_0 \exp\left(-\frac{E_a}{RT}\right) \tag{3-1}$$

where r is the TOF ($mol_{H2}/min/mol_{Cat}$), E_a is the activation energy (kJ/mol), T is the absolute temperature (K) and R is the gas constant (8.3145J/mol/K). From Figure 7c, the calculated activation energy for Ni_5P_4 is 39 kJ/mol, comparable or even smaller than some of reported precious catalysts in Figure 7d (e.g., Pt-Ni@SiO_2 of 54.76[45], Pd-Pt NPs of 51.77[46], $Pt_{0.65}Ni_{0.35}$ of 39[47], Pt-CoCu@SiO_2 of 51.01 eV[41]). This

indicates the potential of this nickel phosphate catalyst for AB hydrolysis.

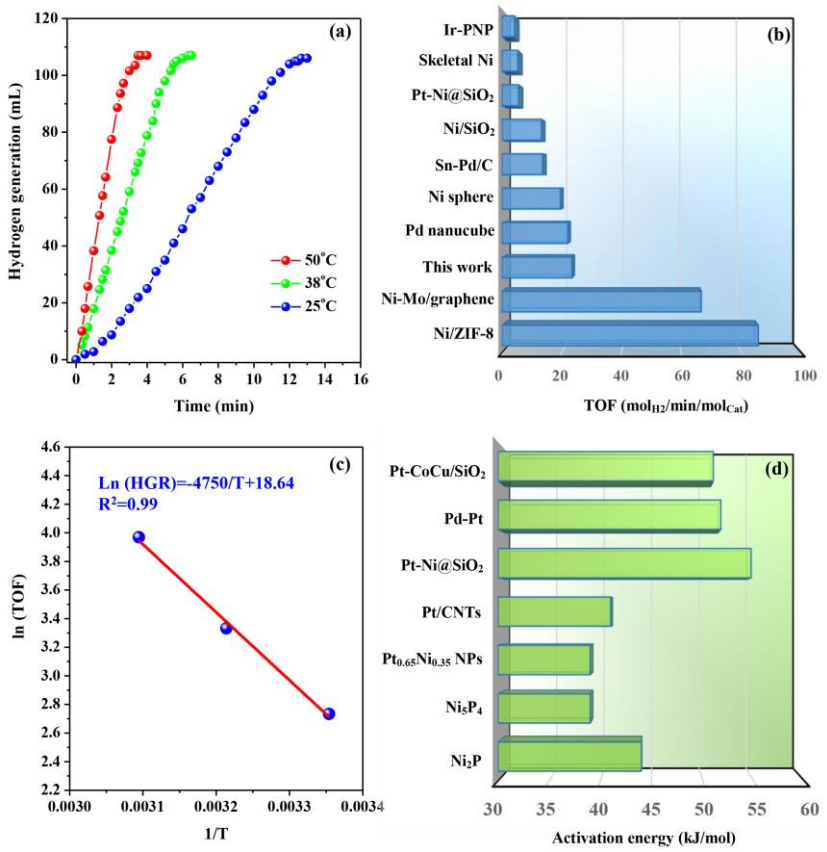

Figure 7 Time courses for H_2 production from hydrolysis of AB using Ni_5P_4 at low n_{Cat}/n_{AB} of 0.02 (a), Arrhenius plot of ln (TOF) versus 1/T (c), comparison of the TOF (b) and activation energy (d) with different reported catalysts.

The durability test of Ni_5P_4 catalyst is performed at room temperature, and shown in Figure 8. It is conducted by the addition of a new proportion of AB solution when the previous run was completed. It can be seen that the Ni_5P_4 catalyst shows good stability and reusability. The high activity after fourth test is still retained. The relatively slower hydrogen generation rate is observed, which could be ascribed to the slight particle agglomeration (Figure S4). This phenomenon is also observed for Ni_2P catalyst[23]. From the above computational and experimental results, it can be seen that manipulating the electron transfer and employing the ensemble effect of P can be effective strategies to enhance the performance of nickel phosphate catalyst for AB

hydrolysis. The results reported herein may pave the way for the rational design of highly efficient nickel phosphate-based catalysts for hydrogen generation.

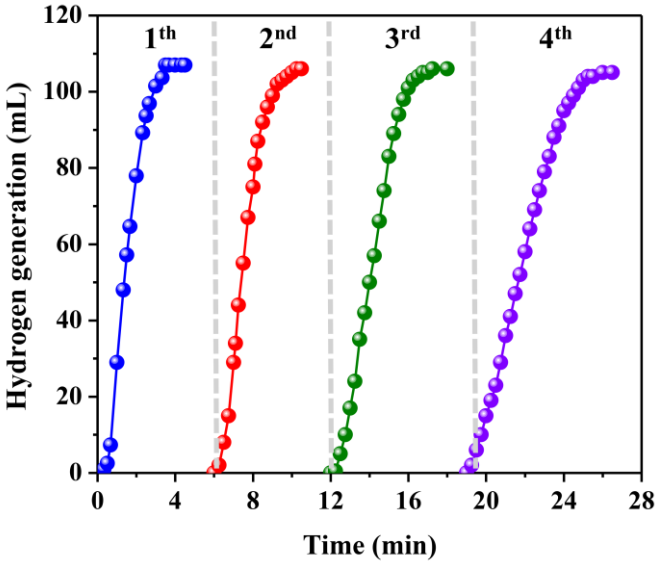

Figure 8 Cycle stability test of Ni_5P_4 for hydrogen generation with the weight of 0.038g. Reaction conditions: 25°C, C_{AB}=0.01g/mL, V_{AB}=5mL.

Conclusions

In summary, the Ni_2P and Ni_5P_4 are synthesized by the phase-controlled thermal decomposition approach and characterized by multi-techniques such as XRD, TEM, XPS. By both DFT calculation and experimental methods, the facilitated electron transfer from Ni to P for Ni_5P_4 than Ni_2P is demonstrated. It is found that Ni_5P_4 catalyst shows impressive catalytic hydrogen evolution rate for ammonia-borane hydrolysis, which is higher than that of Ni_2P catalyst. The activation energy of the Ni_5P_4 catalyst for the hydrolysis of AB is calculated to be 39 kJ/mol, smaller than part of precious metal catalyst. This could be ascribed to the higher positive charge of Ni together with the stronger ensemble effect.

Acknowledgments

This work is financially supported by the National Natural Science Foundation of China (21606254), Natural Science Foundation of Shandong Province (ZR2016BB16), Key research and development plan of Shandong Province (2017GSF17126), Fundamental Research Funds for the Central Universities (18CX02014A) and Independent innovation foundation of Qingdao (17-1-1-18-jch).

References

[1] Rohani P, Kim S, Swihart MT. Boron nanoparticles for room-temperature hydrogen generation from water. Adv Energy Mater 2016;6:1502550.

[2] Dincer I, Acar C. Review and evaluation of hydrogen production methods for better sustainability. Int J Hydrogen Energy 2015;40:11094-111.

[3] Demirci UB, Miele P. Sodium borohydride versus ammonia borane, in hydrogen storage and direct fuel cell applications. Energy Environ Sci 2009;2:627-37.

[4] Feng X, Song Z, Guo T, Yang R, Liu Y, Chen X, et al. Insights into the effect of surface functional groups on catalytic performance for hydrogen generation from sodium borohydride. RSC Adv 2016;6:113260-66.

[5] Ji J, Duan XZ, Qian G, Zhou XG, Tong GS, Yuan WK. Towards an efficient CoMo/γ-Al_2O_3 catalyst using metal amine metallate as an active phase precursor: Enhanced hydrogen production by ammonia decomposition. Int J Hydrogen Energy 2014;39:12490-98.

[6] Wang X, Kolen'ko YV, Bao XQ, Kovnir K, Liu L. One-step synthesis of self-supported nickel phosphide nanosheet array cathodes for efficient electrocatalytic hydrogen generation. Angew Chem Int Ed 2015;54:8188-92.

[7] Xia B, Liu C, Wu H, Luo W, Cheng G. Hydrolytic dehydrogenation of ammonia borane catalyzed by metal-organic framework supported bimetallic RhNi nanoparticles. Int J Hydrogen Energy 2015;40:16391-7.

[8] Gutowska A, Li L, Shin Y, Wang CM, Li XS, Linehan JC, et al. Nanoscaffold mediates hydrogen release and the reactivity of ammonia borane. Angew Chem Int Ed 2005;44:3578-82.

[9] Keaton RJ, Blacquiere JM, Baker RT. Base metal catalyzed dehydrogenation of ammonia−borane for chemical hydrogen storage. J Am Chem Soc 2007;129:1844-5.

[10] Bluhm ME, Bradley MG, Butterick R, Kusari U, Sneddon LG. Amineborane-based chemical hydrogen storage: enhanced ammonia borane dehydrogenation in ionic liquids. J Am Chem Soc 2006;128:7748-9.

[11] Chandra M, Xu Q. A high-performance hydrogen generation system: transition metal-catalyzed dissociation and hydrolysis of ammonia–borane. J Power Sources 2006;156:190-4.

[12] Wang S, Zhang D, Ma Y, Zhang H, Gao J, Nie Y, et al. Aqueous Solution Synthesis of Pt–M (M= Fe, Co, Ni) Bimetallic Nanoparticles and Their Catalysis for the Hydrolytic Dehydrogenation of Ammonia Borane. ACS Appl Mater Interfaces 2014;6:12429-35.

[13] Zhang Z, Lu Z-H, Chen X. Ultrafine Ni–Pt alloy nanoparticles grown on graphene as highly efficient catalyst for complete hydrogen generation from hydrazine borane. ACS Sus Chem Eng 2015;3:1255-61.

[14] Wang L, Li H, Zhang W, Zhao X, Qiu J, Li A, et al. Supported Rhodium Catalysts for Ammonia–Borane Hydrolysis: Dependence of the Catalytic Activity on the Highest Occupied State of the Single Rhodium Atoms. Angew Chem Int Ed 2017;56:4712-8.

[15] Shen J, Yang L, Hu K, Luo W, Cheng G. Rh nanoparticles supported on graphene as efficient catalyst for hydrolytic dehydrogenation of amine boranes for chemical hydrogen storage. Int J Hydrogen Energy 2015;40:1062-70.

[16] Du C, Ao Q, Cao N, Yang L, Luo W, Cheng G. Facile synthesis of monodisperse ruthenium nanoparticles supported on graphene for hydrogen generation from hydrolysis of ammonia borane. Int J Hydrogen Energy 2015;40:6180-7

[17] Chen W, Ji J, Feng X, Duan X, Qian G, Li P, et al. Mechanistic Insight into Size-Dependent Activity and Durability in Pt/CNT Catalyzed Hydrolytic Dehydrogenation of Ammonia Borane. J Am Chem Soc 2014;136:16736-9.

[18] Yan H, Lin Y, Wu H, Zhang W, Sun Z, Cheng H, et al. Bottom-up precise synthesis of stable platinum dimers on graphene. Nature Comm 2017;8:1070.

[19] Wang C, Tuninetti J, Wang Z, Zhang C, Ciganda R, Salmon L, et al. Hydrolysis of Ammonia-Borane over Ni/ZIF-8 Nanocatalyst: High Efficiency, Mechanism, and Controlled Hydrogen Release. J Am Chem Soc 2017;139:11610-5.

[20] Hou CC, Li Q, Fu WF, López N, Chen Y, et al. Ternary Ni-Co-P nanoparticles as noble-metal-free catalysts to boost the hydrolytic dehydrogenation of ammonia-borane. Energy Environ Sci 2017;10: 1770-6.

[21] Men Y, Su J, Du X, Liang L, Cheng G, Luo W. CoBP nanoparticles supported on three-dimensional nitrogen-doped graphene hydrogel and their superior catalysis for hydrogen generation from hydrolysis of ammonia borane. J Alloys Comp 2018;735:1271-6.

[22] Yao Q, Lu Z-H, Huang W, Chen X, Zhu J. High Pt-like activity of the Ni–Mo/graphene catalyst for hydrogen evolution from hydrolysis of ammonia borane. J Mater Chem A 2016;4:8579-83.

[23] Peng CY, Kang L, Cao S, Chen Y, Lin ZS, Fu WF. Nanostructured Ni_2P as a Robust Catalyst for the Hydrolytic Dehydrogenation of Ammonia-Borane. Angew Chem Int Ed 2015;54:15725-9.

[24] Pan Y, Liu Y, Zhao J, Yang K, Liang J, Liu D, et al. Monodispersed nickel phosphide nanocrystals with different phases: synthesis, characterization and electrocatalytic properties for hydrogen evolution. J Mater Chem A 2015;3:1656-65.

[25] Ren J, Wang JG, Li JF, Li YW. Density functional theory study on crystal nickel phosphides. J Fuel Chem Tech 2007;35:458-64.

[26] Moon JS, Kim EG, Lee YK. Active sites of Ni_2P/SiO_2 catalyst for hydrodeoxygenation of guaiacol: A joint XAFS and DFT study. J Catal 2014;311:144-52.

[27] Mulliken RS. Electronic population analysis on LCAO–MO molecular wave functions. I. The J Chem Phys 1955;23:1833-40.

[28] Segall M, Shah R, Pickard C, Payne M. Population analysis of plane-wave electronic structure calculations of bulk materials. Phys Rev B 1996;54:16317.

[29] Du X, Yang C, Zeng X, Wu T, Zhou Y, Cai P, Cheng HZ, Luo W. Amorphous NiP supported on rGO for superior hydrogen generation from hydrolysis of ammonia borane. Int J Hydrogen Energy 2017;42:14181-7.

[30] Du Y, Liu C, Cheng G, Luo W. Cuboid Ni_2P as a Bifunctional Catalyst for Efficient Hydrogen Generation from Hydrolysis of Ammonia Borane and Electrocatalytic Hydrogen Evolution. Chem - Asian J 2017;12:2967-72.

[31] Chang J, Feng L, Liu C, Xing W, Hu X. An Effective Pd–Ni_2P/C Anode Catalyst for Direct Formic Acid Fuel Cells. Angew Chem Int Ed 2014;53:122-6.

[32] Rundqvist S, Lundvik L, Hassler E. Refinement of Ni_3P Structure. Acta Chem Scand 1962. p. 242.

[33] Elfström M. Physical properties of lower nickel phosphides. Acta Chem Scand 1965;19:1694.

[34] Shi Y, Xu Y, Zhuo S, Zhang J, Zhang B. Ni_2P nanosheets/Ni foam composite electrode for long-lived and pH-tolerable electrochemical hydrogen generation. ACS Appl Mater Interfaces 2015;7:2376-84.

[35] Pu Z, Liu Q, Tang C, Asiri AM, Sun X. Ni_2P nanoparticle films supported on a Ti plate as an efficient hydrogen evolution cathode. Nanoscale 2014;6:11031-4.

[36] Sawhill SJ, Layman KA, Van Wyk DR, Engelhard MH, Wang C, Bussell ME. Thiophene hydrodesulfurization over nickel phosphide catalysts: effect of the precursor composition and support. J Catal 2005;231:300-13.

[37] Cecilia J, Infantes-Molina A, Rodríguez-Castellón E, Jiménez-López A. A novel method for preparing an active nickel phosphide catalyst for HDS of dibenzothiophene. J Catal 2009;263:4-15.

[38] Wu C, Kopold P, Aken PAv, Maier J, Yu Y. High Performance Graphene/Ni_2P Hybrid Anodes for Lithium and Sodium Storage through 3D Yolk-Shell-Like Nanostructural Design. Adv Mater 2017;29:1604015.

[39] Zhan WW, Zhu QL, Xu Q. Dehydrogenation of ammonia borane by metal nanoparticle catalysts.

ACS Catal 2016;6:6892-905.

[40] Liao J, Lu D, Diao G, Zhang X, Zhao M, Li H. $Co_{0..8}Cu_{0.2}MoO_4$ microspheres composed of nanoplatelets as a robust catalyst for the hydrolysis of ammonia borane. ACS Sus Chem Eng 2018. DOI: 10.1021/acssuschemeng.7b03994.

[41] Ge Y, Shah Z H, Lin X J, Lu R, Liao Z, Zhang S. Highly efficient Pt decorated CoCu bimetallic nanoparticles protected in silica for hydrogen production from ammonia-borane. ACS Sus Chem Eng 2016;5:1675-1684.

[42] Durap F, Zahmakıran M, Ozkar S, Water soluble laurate-stabilized ruthenium (0) nanoclusters catalyst for hydrogen generation from the hydrolysis of ammonia-borane: High activity and long lifetime. Int J Hydrogen Energy 2009;34:7223-72230.

[43] Li Y, Dai Y, Tian X K. Controlled synthesis of monodisperse Pd_xSn_{100-x} nanoparticles and their catalytic activity for hydrogen generation from the hydrolysis of ammonia-borane. Int J Hydrogen Energy 2015;40:9235-9243.

[44] Tang C, Xie L, Wang K, Du G, Asiri AM, Luo Y, et al. A Ni_2P nanosheet array integrated on 3D Ni foam: an efficient, robust and reusable monolithic catalyst for the hydrolytic dehydrogenation of ammonia borane toward on-demand hydrogen generation. J Mater Chem A 2016;4:12407-10.

[45] Qi X, Li X, Chen B, Lu H, Wang L, He G. Highly active nanoreactors: patchlike or thick Ni coating on Pt nanoparticles based on confined catalysis. ACS Appl Mater Interfaces 2016;8:1922-8.

[46] Amali A J, Aranishi K, Uchida T, Xu Q. PdPt nanocubes: A high-performance catalyst for hydrolytic dehydrogenation of ammonia borane. Part Part Syst Charact 2013;30:888-92.

[47] Yang X, Cheng F, Liang J, Tao Z, Chen J. Pt_xNi_{1-x} nanoparticles as catalysts for hydrogen generation from hydrolysis of ammonia borane. Inter J Hydrogen Energy 2009;34:8785-91.